Solar Energy 145 (2017) 52–58

Contents lists available at ScienceDirect

Solar Energy

journal homepage: www.elsevier.com/locate/solener

Simulations of chalcopyrite/c-Si tandem cells using SCAPS-1D

Kihwan Kim, Jihye Gwak *, Seung Kyu Ahn, Young-Joo Eo, Joo Hyung Park, Jun-Sik Cho, Min Gu Kang, Hee-Eun Song, Jae Ho Yun *

Photovoltaic Laboratory, Korea Institute of Energy Research, Daejeon 34129, Republic of Korea

ARTICLE INFO

Article history:
Received 4 January 2016
Received in revised form 29 December 2016
Accepted 12 January 2017
Available online 26 January 2017

Keywords:
Multi-junction
Tandem
SCAPS-1D
Simulation
CIGS
Si

ABSTRACT

In this work, we present SCAPS-1D simulations of dual-junction tandem cells with chalcopyrite top subcells with various bandgaps (E_g = 1.4, 1.5, 1.6, and 1.7 eV) and a c-Si bottom subcell. The purpose of these simulations is to assess achievable device performances with a CIGS/c-Si tandem structure when a realistic efficiency of each subcell is applied. The top subcell conditions are simulated based on the state-of-the-art records, and the bottom c-Si cell is designed to have an efficiency of approximately 19%. When the E_g of the top chalcopyrite cell is below 1.5 eV, the current matching condition between the top cell and bottom cell is not obtained until the top cell's thickness is 0.2 μm. However, with E_g values of the top chalcopyrite cells at 1.6 eV and 1.7 eV, the current matching conditions could be found. Nevertheless, because the efficiency from the top chalcopyrite cell is approximately 12%, it is predicted that the tandem structure exhibits a similar device performance to the bottom c-Si cell. This result suggests that improving the efficiency of the wide bandgap cell is essential for the tandem cell to overcome the efficiency form a single-junction solar cell.

1. Introduction

The efforts to surpass the efficiency of a solar cell with a single junction have led to numerous trials to fabricate multi-junction cells (tandem cells) comprised of solar cells with different bandgaps (Luque and Marti, 2010; Friedman et al., 2010). This technique provides a potentially higher conversion efficiency because serially connected junctions with different bandgaps absorb a greater range of photons with less energy loss. Theoretically, an infinite stack of junctions can have an efficiency of 65.4% under AM 1.5 illumination, and even further improvement in performance is possible using a concentrated incident spectrum (Martí and Araújo, 1996). In particular, applications of this technique to III-V or a-Si solar cells have been successfully demonstrated for several decades (Dimroth et al., 2014; Chiu et al., 2014; Sasaki et al., 2013; Press release of Fraunhofer-Institut für Solare Energiesysteme, 2014; Ahn et al., 2012).

In contrast to III-V or a-Si solar cells, few studies on chalcopyrite ($Cu(In,Ga)Se_2$, CIGS for short)-based tandem solar cells have been performed, despite chalcopyrite materials having tunable bandgaps ranging from 1.0 eV to 1.7 eV (Shafarman et al., 2010; Shafarman and Paulson, 2005). A theoretical calculation predicts an efficiency of 28% from 2 junctions with a controlled combination of bandgaps (Coutts et al., 2003). However, serial stacking of two chalcopyrite absorber layers is practically difficult because the bottom subcell undergoes a significant degradation in its original device performance due to the high process temperature of the top subcell fabrication (Shafarman and Paulson, 2005). To date, to the best of our knowledge, no monolithically stacked CIGS tandem cell (i.e., not a mechanically stacked multi-junction cell (Nishiwaki et al., 2003) has reported a better device performance compared to an optimized single-junction device. Recently, hybrid multi-junction cells consisting of low-temperature grown top subcells and bottom CIGS solar cells have also been extensively studied because this approach offers a relatively wide process window for the cell stacking (Liska et al., 2006; Bailie et al., 2015; Kosyachenko et al., 2015); nevertheless, the obtained device performance from the hybrid multi-junction cells do not appear to compensate for the effort required to make the multi-junction devices.

Another means to demonstrate a tandem solar cell is to combine a top wide-bandgap CIGS solar cell with a bottom conventional Si-based solar cell (White et al., 2014). This approach has not yet realized an improved device performance compared to an optimized single junction CIGS device, but it appears to be more practical than the all-chalcopyrite tandem cell approach because the conventional Si-based solar cells have not only high efficiencies in excess of 20% (Masuko et al., 2014) but also better thermal stability.

* Corresponding authors.
E-mail addresses: bleucoeur@kier.re.kr (J. Gwak), yunjh92@kier.re.kr (J.H. Yun).

http://dx.doi.org/10.1016/j.solener.2017.01.031
0038-092X/

Nomenclature

J_{SC}	short-circuit current density, mA/cm^2	η	conversion efficiency, %
V_{OC}	open-circuit voltage, V	J_{MPP}	current density at the maximum power point
FF	fill factor, %		

In this work, we present simulations of (dual-junction) tandem cell with a chalcopyrite top cell ($E_g \geqslant 1.4$ eV) and a c-Si bottom cell using the SCAPS-1D (Solar Cell Capacitance Simulator – 1D) simulation tool (Burgelman et al., 2000). First, wide-bandgap CIGS solar cells ($E_g \geqslant 1.4$ eV) were simulated to fit the state-of-the-art data reported thus far, and then, a c-Si solar cell was simulated to have an efficiency of 18–19%. With the thinning of the absorber layer of the top subcells (i.e., wide-bandgap CIGS solar cells), the current matching conditions were determined to enable both the top and bottom subcells to have the same J_{MPP} or J_{SC} values. The obtained results suggested that the E_g of the top subcell must be greater than or equal to 1.6 eV (among the sample set in the present study) to obtain the current matching condition while ensuring a practical top-subcell layer thickness. Nevertheless, the simulation indicated that the tandem solar cell does not provide a substantial benefit in terms of the device performance. The relatively lower efficiencies from the top CIGS subcells limit the device performances of the tandem solar cells. Thus, improvement of efficiencies of wide-bandgap CIGS solar cells must be undertaken beforehand to demonstrate a CIGS/c-Si tandem solar cell that exceeds the device performance from an optimized single-junction device.

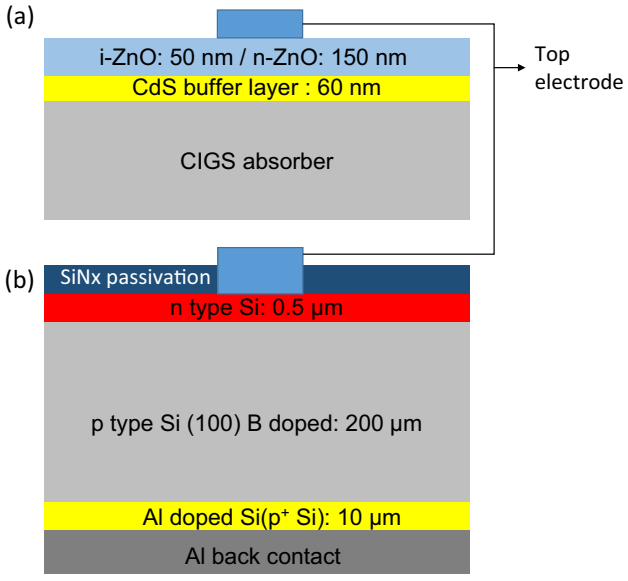

Fig. 1. Schematic diagrams of a CIGS solar cell and a c-Si solar cell.

2. Methods

First, we assumed that the CIGS/c-Si tandem solar cells have an ideal tunnel junction, having neither electrical resistance nor optical loss, between the top and bottom subcells. The current matching conditions were examined by adjusting the thickness of the CIGS solar cells (i.e., the top subcell). We also assumed that the optical loss in each interface is negligible. Because the SCAPS-1D simulation tool does not fully support a solar cell with a multi-junction structure, by simulating top and bottom subcells separately, the current matching conditions were obtained.

The simulations of the top CIGS (Eg = 1.4, 1.5, 1.6, and 1.7 eV) subcells are mostly based on the NUMOS model (Burgelman et al., 2007; Decock et al., 2011), which is one of the default models in the SCAPS-1D simulation package; the structure of the CIGS solar cell is shown in Fig. 1(a). The absorption coefficients of the CIGS absorber layers (Eg = 1.4, 1.5, 1.6, and 1.7 eV) were calculated from interpolation of measured optical constants reported by P. D. Paulson and coworkers (Paulson et al., 2003). In addition, to adjust the calculated absorption coefficients realistically, the absorption coefficients corresponding the sub-bandgap range were also corrected. Table 1 lists the basic input values for the top CIGS subcells' simulations. We also assumed that the CIGS solar cells do not have an internal bandgap gradient. To simulate a c-Si subcell for the bottom subcell, in-house data were used (Jeong et al., 2014; Do et al., 2014). The simulations were performed to generate a c-Si solar cell with efficiency of 18–19%. The schematic diagram and input values of the c-Si solar cells are also given in Fig. 1(b) and Table 1.

Finding the current matching point between the two subcells is straightforward. With thinning of the top cell's absorber layer, the J_{MPP} and J_{SC} of the top CIGS subcell and the transmitted light through the top CIGS subcell were calculated. The transmitted light spectrum, $S(\lambda)$, is given by

Table 1
Input parameters for SCAPS-1D simulation.

	CIGS E_g = 1.4 eV	CIGS E_g = 1.5 eV	CIGS E_g = 1.6 eV	CIGS E_g = 1.7 eV	n + Si	p-Si	p + Si
Thickness (μm)	Variable	Variable	Variable	Variable	0.5	200	10
E_g (eV)	1.4	1.5	1.6	1.7	1.12	1.12	1.12
n (cm^{-3})	1.0E+00	1.0E+00	1.0E+00	1.0E+00	1.0E+20	1.0E+16	5.0E+18
p (cm^{-3})	5.0E+15	1.0E+16	5.0E+15	5.0E+15	1.0E+01	1.0E+01	1.0E+01
Bulk defect type	Neutral	Neutral	Neutral	Neutral	Neutral	Neutral	Neutral
Bulk defect (cm^{-3}, above E_{V_CIGS})	2.0E14 at 0.3 eV 1.0E14 at 0.8 eV	1.0E15 at 0.8 eV	1.0E15 at 0.8 eV	1.0E15 at 0.8 eV	5.0E14 at 0.6 eV	4.0E12 at 0.6 eV	4.0E14 at 0.6 eV
Interface defect	N/A	CdS/CIGS (neutral)	CdS/CIGS (neutral)	CdS/CIGS (neutral)	N/A	N/A	N/A
Interface defect (cm^{-2}, above E_{V_CIGS})	N/A	1.0E11 at 0.6 eV	1.0E11 at 0.6 eV	1.0E10 at 0.6 eV	N/A	N/A	N/A

$$S(\lambda) = S_o(\lambda) \cdot \exp(-\alpha_{ZnO}(\lambda) \cdot d_{ZnO}) \cdot \exp(-\alpha_{CdS}(\lambda) \cdot d_{CdS}) \cdot \exp(-\alpha_{CIGS}(\lambda) \cdot d_{CIGS}), \quad (1)$$

where S_o is the incident light spectrum, α is the absorption coefficient of a material, and d is the thickness of a material. The reflection losses from each interface were not taken into account.

Next, the transmitted light spectra were used as the input light spectra of the bottom c-Si subcell. Finally, the J_{MPP} and J_{SC} values of the c-Si subcell were calculated. The absorber thickness of the top CIGS subcell was limited to 0.2 μm in the simulation, given that it is practically difficult to maintain the device properties of a thin absorber layer with thickness less than 0.2 μm (Lundberg et al., 2003; Kim et al., 2013).

3. Results and discussion

3.1. Top-subcell simulations

The simulations of CIGS solar cells were performed mostly based on the NUMOS model. Only the absorption profiles were obtained from P. D. Paulson's study (Paulson et al., 2003). Fig. 2 shows the J-V curves of CIGS solar cells for the top-subcells, and their J-V characteristics are given in Table 2. The CIGS solar cells with E_g = 1.4, 1.5 and 1.6 eV do not exhibit large differences in the V_{OC}, which reflects the real data obtained to date (Contreras et al., 2012). In addition, the simulated V_{OC} of the CIGS solar cells are slightly smaller than the real data because we assumed the CIGS absorber layers do not have internal bandgap gradients (Hanket et al., 2009; Kim et al., 2015). If a CIGS solar cell has a wider bandgap near the CdS/CIGS interface, then a higher V_{OC} is expected (Kim et al., 2015). However, to induce the current matching condition between the top subcell and bottom subcell, the top CIGS solar cells should be thinner than the normal absorber layer (i.e., 2 μm). In such a case, the internal bandgap gradients make the simulation complicated; furthermore, when the CIGS absorber layers are thin, it becomes ambiguous to choose the representative bandgaps of the CIGS absorber layers.

Fig. 3 presents the external quantum efficiency (EQE) curves (a) of the CIGS solar cells shown in Fig. 2 and their first derivative with respect to wavelength (b). The obtained simulations reveal that the CIGS solar cells with various bandgaps do not exhibit any significant difference in the short wavelength region (i.e., <500 nm). Only the cutoffs of the EQE curves of each bandgap move toward the short wavelength in accordance with their bandgaps. Fig. 3(b) shows the first derivatives of the EQE curves with respect to wavelength, where the local minima provide approximations of the bandgaps. The CIGS solar cells with nominal bandgaps = 1.4, 1.5, 1.6 and 1.7 eV are estimated to have bandgaps of 1.38, 1.48, 1.59, and 1.69 eV, respectively, suggesting that the absorption profiles approximated from P. D. Paulson's study (Paulson et al., 2003) fit properly.

Chalcopyrite materials are known to have quite a high absorption coefficient, and thus, the top subcell thinning process is

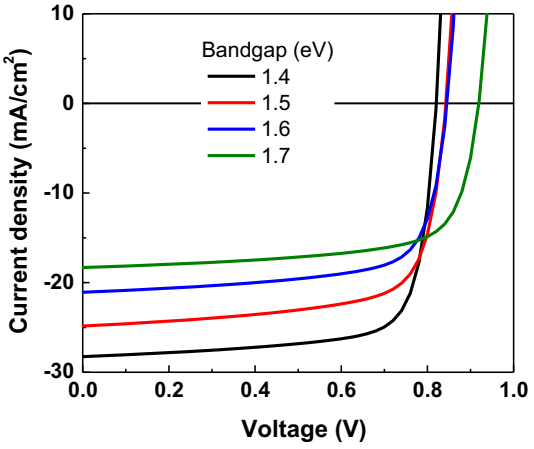

Fig. 2. Simulated J-V curves of the CIGS subcells.

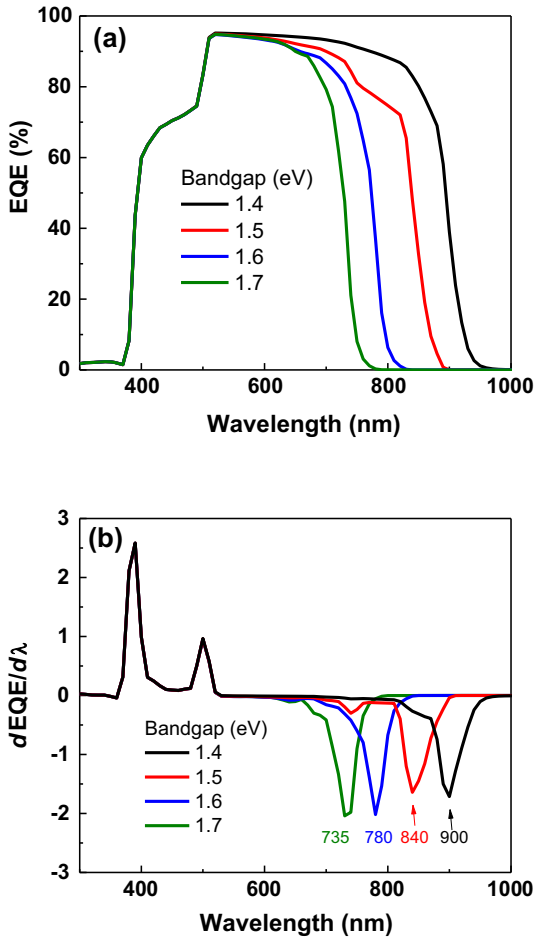

Fig. 3. (a) EQE curves of simulated CIGS subcells and (b) their first derivatives with respect to wavelength.

Table 2
Light J-V characteristics of the CIGS solar cells shown in Fig. 2.

Top cell bandgap (eV)	Voc (V)	Jsc (mA/cm^2)	FF (%)	η (%)	V_{MPP} (V)	J_{MPP} (mA/cm^2)
1.4	0.831	28.2	76.9	18.0	0.723	24.9
1.5	0.843	24.6	71.3	14.8	0.722	20.5
1.6	0.845	20.9	71.5	12.6	0.725	17.4
1.7	0.917	18.0	69.1	11.4	0.783	14.5

indispensable to ensure the current matching condition with the bottom c-Si solar cell. Fig. 4 shows illuminated J-V characteristics with respect to the thickness of the top CIGS solar cell. First, the efficiencies of the CIGS solar cells remain almost constant until a thickness of 0.5 μm (see Fig. 4(a)). However, beyond this point (i.e., less than 0.5 μm), the efficiencies begin to decline, mostly due to the decrease in J_{SC} (see Fig. 4(b)). In fact, incomplete light absorption occurs even when the CIGS thickness is less than 1 μm. However, the fill factor improvement with the CIGS absorber thinning compensates the loss from the incomplete light absorption (see Fig. 4(d)). Thus, the decline of the efficiencies is only evident for absorber layers thinner than 0.5 μm. The reason for the fill factor improvement is based on the reduction of SRH recombination. For example, a CIGS solar cell (E_g = 1.7 eV) with a thickness of 1.0 μm have approximately 35% greater SRH recombination current than that with a thickness of 0.25 μm at V = 0 V. Basically, the SRH recombination reduction is attributed to the decrease of the device volume. Consequently, it helps to maintain V_{OC} even when the absorber thickness is considerably thinner than a normal thickness (i.e., ⩾1 μm). The fill factor improvement (or maintaining V_{OC}) seems to be uncommonly observed; however, there are several previous works reporting solar cells with a thin absorber that maintain a similar (even improved) fill factor and/or V_{OC} (Lundberg et al., 2003; Kim et al., 2013; Kim and Shafarman, 2016; Smestad and Ries, 1992). Nevertheless, these simulation results are built on the assumption that the thickness of a CIGS absorber does not affect any of shunting, recombination mechanisms, or interfaces. As a result, the CIGS solar cells with thin absorber layers (i.e., <1 μm) preserve their device behaviors compared to cells with normal absorber layer thicknesses (i.e., ⩾1 μm).

3.2. Bottom-subcell simulations

In this work, a c-Si solar cell with a typical performance was employed as the bottom-subcell in the tandem solar cell. More specifically, this simulation of the c-Si solar cell is modeled after an in-house c-Si solar cell, which exhibits an efficiency of 18.7% with V_{OC} = 637 mV, J_{SC} = 37.2 mA/cm^2, and fill factor = 78.9% (Jeong et al., 2014). The structure and device fabrication procedure are described in detailed in elsewhere (Do et al., 2014; Lee et al., 2015). Basically, the simulation of the c-Si solar cells is mostly based on the default parameters provided with the SCAPS-1D; the charge carrier densities of each layer are measured values. However, to account for optical loss from the SiN_x passivation layer, a measured absorption profile was incorporated into the simulation. Fig. 5 presents the simulated J-V curve of the c-Si solar cell. The simulated device exhibits an efficiency of 18.7% with V_{OC} = 639 mV, J_{SC} = 36.9 mA/cm^2, and fill factor = 79.4%, indicating that the difference between the real and simulated results is insignificant.

3.3. Tandem cell simulations

A straightforward strategy was used to simulate CIGS/c-Si tandem solar cells. First, light transmission through the top CIGS subcells were calculated using each layer's absorption profiles, and

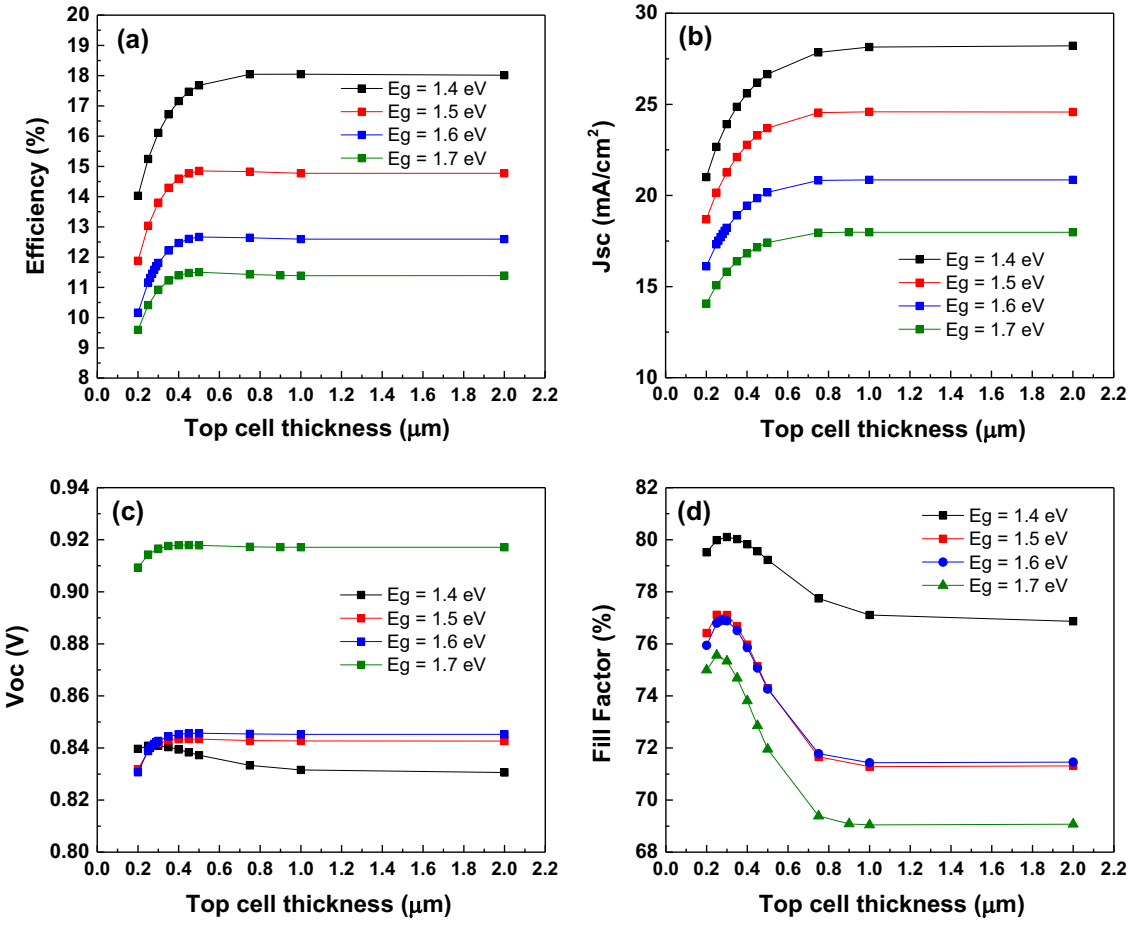

Fig. 4. Simulated light J-V characteristics with respect to the absorber thickness: (a) efficiency, (b) J_{SC}, (c) V_{OC}, and (d) FF.

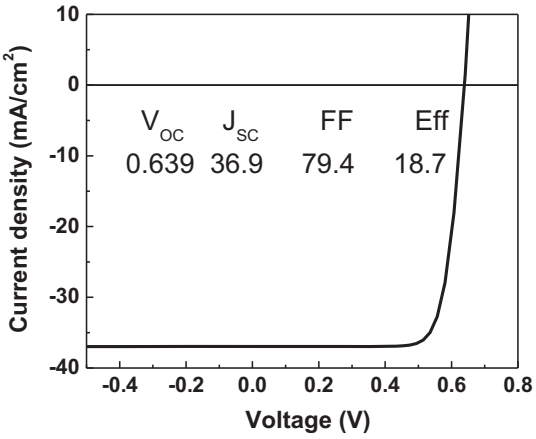

Fig. 5. Simulated J-V curve of a c-Si solar cell.

then the transmitted light spectra were used as the incident light of the bottom c-Si subcells.

In the present study, the current matching condition is defined as the condition where the top and bottom subcells have either the same J_{MPP} or J_{SC} value. In other words, each combination of CIGS/c-Si tandem cells can achieve up to two current matching conditions. Some previous studies only defined the current matching condition using the J_{SC} (Elbar et al., 2015; Ho Song et al., 2015). However, using J_{MPP} can be more advantageous in the present study because the bottom c-Si solar cell has a significantly greater fill factor than the top CIGS subcells. By allowing the currents of the two subcells to have the same J_{MPP}, a greater fill factor from the tandem solar cell can be obtained in this study (Friedman et al., 2010). In addition, further top-subcell-thinning should be performed to match the same J_{SC} from the top and bottom subcells. If the top and bottom subcells have similar fill factors (e.g., III-V tandem cells), then both approaches (i.e., matching J_{SC} vs. matching J_{MPP}) should provide similar results. Thus, both the cases should be examined.

Fig. 6 displays the J_{MPP} and J_{SC} values of the top and bottom subcells with respect to the thicknesses of the CIGS absorber in the top subcells. First, the CIGS solar cells with E_g = 1.4 and 1.5 eV failed to meet the current matching condition until the CIGS absorber thickness = 0.2 μm. However, the 1.6-eV-CIGS solar cells with absorber thickness = 0.27 and 0.24 μm were found to have both of the J_{MPP} and J_{SC} current matching conditions with the bottom c-Si solar cells, respectively. Not surprisingly, the 1.7-eV-CIGS solar cell was also found to have two current matching points with the bottom c-Si solar cell at J_{MPP} = 14.5 mA/cm^2 (thickness = 1.0 μm) and J_{SC} = 17.1 mA/cm^2 (thickness = 0.44 μm).

With the current matching conditions above, CIGS/c-Si tandem solar cells were simulated; their J-V characteristics are given in Fig. 7 and Table 3. The construction of J-V curves of the tandem solar cells is based on the assumption that the lower-current subcell dominates the JV characteristic of a tandem solar cell (Kurtz et al., 1994). The simulated results revealed all of the combinations (i.e., Fig. 7(a)–(d)) exhibit similar conversion efficiencies of approximately 19–20%, indicating that the tandem devices do not significantly exceed the device performance of an optimized single-junction CIGS solar cell. Considering practical issues, the

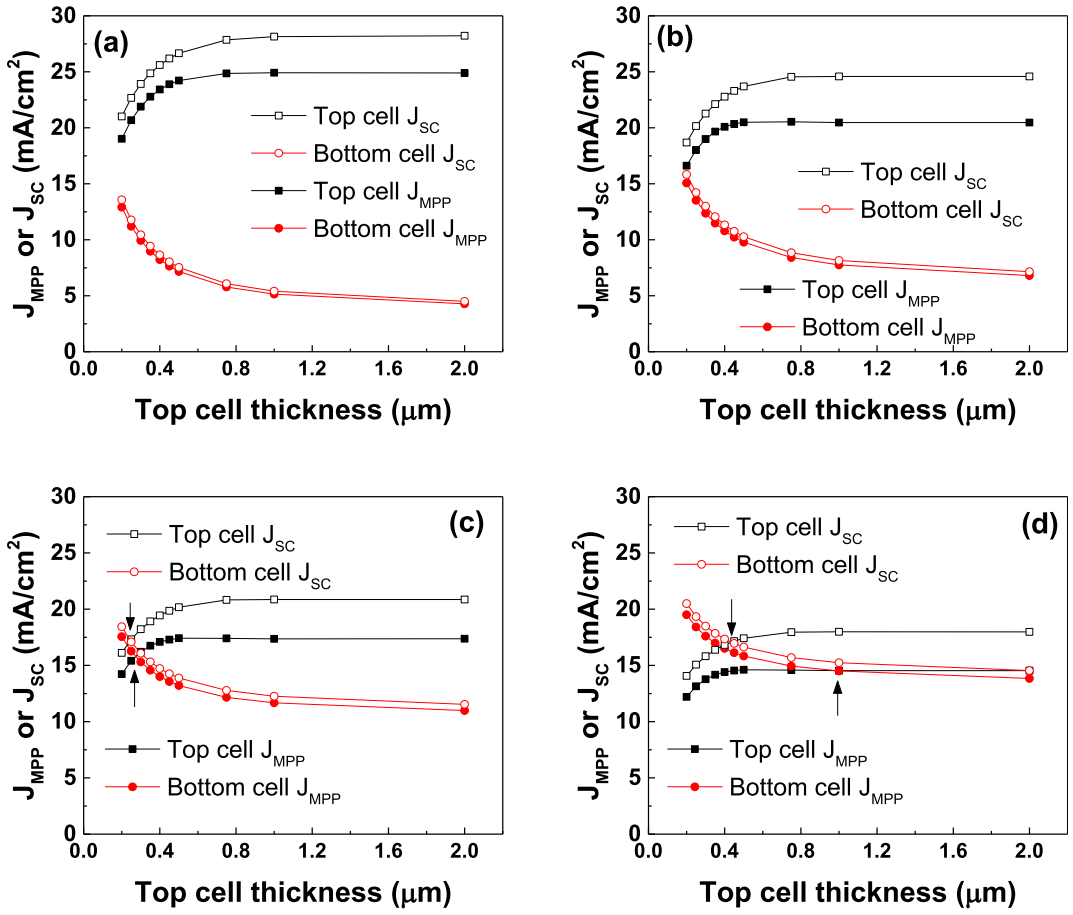

Fig. 6. J_{MPP} and J_{SC} Comparisons between the top- and bottom-subcells. Top CIGS subcell bandgap: (a) 1.4 eV; (b) 1.5 eV; (c) 1.6 eV; and (d) 1.7 eV. The current matching points are indicated with arrows.

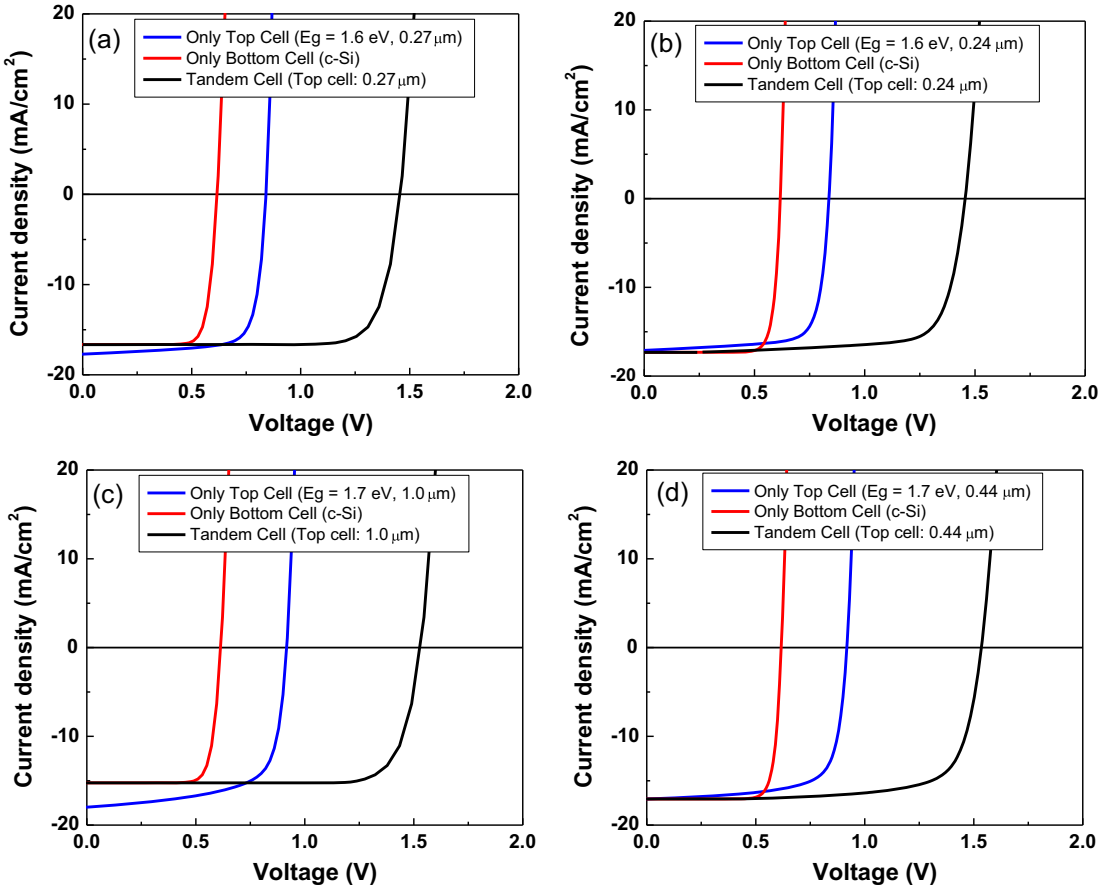

Fig. 7. Light J-V curves of tandem CIGS/c-Si solar cells. Bandgap of the top CIGS subcell = 1.6 eV: (a) J_{MPP}- and (b) J_{SC}-matching conditions; Bandgap of the top CIGS subcell = 1.7 eV: (c) J_{MPP}- and (d) J_{SC}-matching conditions.

Table 3
Light J-V characteristics of the CIGS/c-Si tandem solar cells shown in Fig. 7.

Top cell condition	Voc (V)	Jsc (mA/cm^2)	FF (%)	η (%)	V_{MPP} (V)	J_{MPP} (mA/cm^2)
(a) 1.6 eV (t = 0.27 μm)	1.454	16.7	81.5	19.8	1.253	15.8
(b) 1.6 eV (t = 0.24 μm)	1.455	17.3	77.1	19.4	1.258	15.4
(c) 1.7 eV (t = 1.0 μm)	1.526	15.2	81.9	19.0	1.310	14.5
(d) 1.7 eV (t = 0.44 μm)	1.535	17.1	74.7	19.6	1.323	14.8

engineering window must be far narrower than that expected from the present study. One of the major concerns not discussed here is the optical losses that inevitably occur at each interface and layer. In the present study, only absorption in each layer is taken into account; however, other optical loss factors, such as reflection and haze, must deteriorate light transmission, suggesting the optical design of tandem solar cells should be more sophisticated. Nevertheless, to guarantee the appropriateness for the pursuit of CIGS/c-Si tandem solar cells, improving the top-cell efficiencies should be addressed. To obtain a 25% efficient CIGS/c-Si tandem solar cell (without improving the bottom cell's efficiency), a $\geqslant$ 17%-efficient wide bandgap CIGS solar cell (Eg $\geqslant$ 1.6 eV), should first be demonstrated.

4. Conclusions

Tandem solar cells consisting of top CIGS and bottom c-Si subcells were computationally examined using the SCAPS-1D simulation tool. First, CIGS solar cells (top subcell) of various bandgaps (i.e., 1.4, 1.5, 1.6, and 1.7 eV) having state-of-the-art efficiencies and a conventional c-Si solar cell (bottom subcell) were simulated separately. Next, with CIGS absorber thinning, the current matching condition with the bottom c-Si subcell was examined. The CIGS subcells with Eg = 1.4 and 1.5 eV were found to not achieve the current matching condition until thickness = 0.2 μm. Tandem devices with top CIGS subcells having E_g = 1.6 and 1.7 eV exhibited the current matching conditions before the absorber thickness reached 0.2 μm; nevertheless, these tandem devices were found to have similar device performances compared to the bottom c-Si solar cell. These results indicated that improving the efficiency from the top CIGS subcell is essential to ensure a benefit from the tandem device.

Conflict of interest

The authors declare no competing financial interests.

Acknowledgments

This research was financially supported by the Technology Development Program to Solve Climate Changes of the National Research Foundation (NRF) funded by the Ministry of Science, ICT

& Future Planning (grant no. 2016M1A2A2936753), and the International Collaborative Energy Technology R&D Program (grant no. 20138520011120) and New & Renewable Energy Core Technology Program (grant no. 20153030013080) of the Korea Institute of Energy Technology Evaluation and Planning (KETEP) funded by the Ministry of Trade, Industry & Energy, Republic of Korea.

References

Ahn, S., Lee, S., Lee, H., 2012. Toward commercialization of triple-junction thin-film silicon solar panel with >12% efficiency, presented. In: 27th European Photovoltaic Solar Energy Conference.

Bailie, C.D., Christoforo, M.G., Mailoa, J.P., Bowring, A.R., Unger, E.L., Nguyen, W.H., Burschka, J., Pellet, N., Lee, J.Z., Gratzel, M., Noufi, R., Buonassisi, T., Salleo, A., McGehee, M.D., 2015. Semi-transparent perovskite solar cells for tandems with silicon and CIGS. Energy Environ. Sci. 8, 956–963.

Burgelman, M., Nollet, P., Degrave, S., 2000. Modelling polycrystalline semiconductor solar cells. Thin Solid Films 361, 527–532.

Burgelman, M., Verschraegen, J., Minnaert, B., Marlein, J., 2007. Numerical simulation of thin film solar cells: practical exercises with SCAPS. In: Burgelman, M., Topič, M. (Eds.), Proceedings of NUMOS. University of Gent, pp. 357–366.

Chiu, P.T., Law, D.C., Woo, R.L., Singer, S.B., Bhusari, D., Hong, W.D., Zakaria, A., Boisvert, J., Mesropian, S., King, R.R., Karam, N.H., 2014. Direct semiconductor bonded 5J cell for space and terrestrial applications. IEEE J. Photovoltaics 4, 493–497.

Contreras, M.A., Mansfield, L.M., Egaas, B., Li, J., Romero, M., Noufi, R., Rudiger-Voigt, E., Mannstadt, W., 2012. Wide bandgap Cu(In,Ga)Se_2 solar cells with improved energy conversion efficiency. Prog. Photovoltaics Res. Appl. 20, 843–850.

Coutts, T.J., Ward, J.S., Young, D.L., Emery, K.A., Gessert, T.A., Noufi, R., 2003. Critical issues in the design of polycrystalline, thin-film tandem solar cells. Prog. Photovoltaics Res. Appl. 11, 359–375.

Decock, K., Khelifi, S., Burgelman, M., 2011. Modelling multivalent defects in thin film solar cells. Thin Solid Films 519, 7481–7484.

Dimroth, F., Grave, M., Beutel, P., Fiedeler, U., Karcher, C., Tibbits, T.N.D., Oliva, E., Siefer, G., Schachtner, M., Wekkeli, A., Bett, A.W., Krause, R., Piccin, M., Blanc, N., Drazek, C., Guiot, E., Ghyselen, B., Salvetat, T., Tauzin, A., Signamarcheix, T., Dobrich, A., Hannappel, T., Schwarzburg, K., 2014. Wafer bonded four-junction GaInP/GaAs//GaInAsP/GaInAs concentrator solar cells with 44.7% efficiency. Prog. Photovoltaics Res. Appl. 22, 277–282.

Do, K.S., Baek, T.-H., Kang, M., Choi, S., Kang, G., Yu, G., Lee, J., Myoung, J.-M., Song, H.-E., 2014. Experimental and simulation study for ultrathin (~100 μm) mono crystalline silicon solar cell with 156 × 156 mm^2 area. Met. Mater. Int. 20, 545–550.

Elbar, M., Tobbeche, S., Merazga, A., 2015. Effect of top-cell CGS thickness on the performance of CGS/CIGS tandem solar cell. Sol. Energy 122, 104–112.

Friedman, D.J., Olson, J.M., Kurtz, S., 2010. High-efficiency III-V multijunction solar cells. In: Luque, A., Hegedus, S. (Eds.), Handbook of Photovoltaic Science and Engineering, Chichester, West Sussex, UK, pp. 314–364.

Hanket, G.M., Boyle, J.H., Shafarman, W.N., 2009. Characterization and device performance of (AgCu)(InGa)Se_2 absorber layers. In: Conference Record of 34th IEEE Photovoltaic Specialists Conference, 2009. IEEE, pp. 001240–001245.

Ho Song, S., Aydil, E.S., Campbell, S.A., 2015. Metal-oxide broken-gap tunnel junction for copper indium gallium diselenide tandem solar cells. Sol. Energy Mater. Sol. Cells 133, 133–142.

Jeong, M.S., Kang, M.G., Lee, J.I., Song, H.-E., 2014. Electrode formation using light induced electroless plating in the crystalline silicon solar cells with various anti-reflection coating, presented. In: 4th Asia-Pacific Forum on Renewable Energy Korean Society for New and Renewable Energy, Yeosu, Korea, pp. O-PV-009.

Kim, K., Shafarman, W.N., 2016. Alternative device structures for CIGS-based solar cells with semi-transparent absorbers. Nano Energy 30, 488–493.

Kim, K., Park, H., Kim, W.K., Hanket, G.M., Shafarman, W.N., 2013. Effect of reduced Cu(InGa)$(SeS)_2$ thickness using three-step $H_2Se/Ar/H_2S$ reaction of Cu-In-Ga metal precursor. IEEE J. Photovoltaics 3, 446–450.

Kim, K., Park, H., Hanket, G.M., Kim, W.K., Shafarman, W.N., 2015. Composition and bandgap control in Cu(In,Ga)Se_2-based absorbers formed by reaction of metal precursors. Prog. Photovoltaics Res. Appl. 23, 765–772.

Kosyachenko, L.A., Mathew, X., Maslyanchuk, O.L., Mykytyuk, T.I., Fodchuk, I.M., Kulchynsky, V.V., 2015. Optical characteristics of CdMgTe/Cu(In,Ga)Se_2 two-terminal tandem solar cell. Sol. Energy 116, 399–406.

Kurtz, S.R., Emery, K., Olson, J., 1994. Methods for analysis of two-functional, two-terminal photovoltaic devices. In: Conference Record of the 24th IEEE Photovoltaic Specialists Conference, pp. 1733–1737.

Lee, J.-K., Lee, J.-S., Jang, B.-Y., Kim, J.-S., Ahn, Y.-S., Kang, G.-H., Song, H.-E., Kang, M.-G., Cho, C.-H., 2015. 6″ crystalline silicon solar cell with electron-beam melting-based metallurgical route. Sol. Energy 115, 322–328.

Liska, P., Thampi, K.R., Grätzel, M., Brémaud, D., Rudmann, D., Upadhyaya, H.M., Tiwari, A.N., 2006. Nanocrystalline dye-sensitized solar cell/copper indium gallium selenide thin-film tandem showing greater than 15% conversion efficiency. Appl. Phys. Lett. 88, 203103.

Lundberg, O., Bodegård, M., Malmström, J., Stolt, L., 2003. Influence of the Cu(In,Ga)Se_2 thickness and Ga grading on solar cell performance. Prog. Photovoltaics Res. Appl. 11, 77–88.

Luque, A., Marti, A., 2010. Theoretical limits of photovoltaic conversion and new-generation solar cells. In: Luque, A., Hegedus, S. (Eds.), Handbook of Photovoltaic Science and Engineering, Chichester, West Sussex, UK, pp. 130–168.

Martí, A., Araújo, G.L., 1996. Limiting efficiencies for photovoltaic energy conversion in multigap systems. Sol. Energy Mater. Sol. Cells 43, 203–222.

Masuko, K., Shigematsu, M., Hashiguchi, T., Fujishima, D., Kai, M., Yoshimura, N., Yamaguchi, T., Ichihashi, Y., Mishima, T., Matsubara, N., 2014. Achievement of more than 25% conversion efficiency with crystalline silicon heterojunction solar cell. IEEE J. Photovoltaics 4, 1433–1435.

Nishiwaki, S., Siebentritt, S., Walk, P., 2003. A stacked chalcopyrite thin-film tandem solar cell with 1.2 V open-circuit voltage. Prog. Photovoltaics Res. Appl. 11, 243–248.

Paulson, P.D., Birkmire, R.W., Shafarman, W.N., 2003. Optical characterization of $CuIn_{1-x}Ga_xSe_2$ alloy thin films by spectroscopic ellipsometry. J. Appl. Phys. 94, 879–888.

Press release of Fraunhofer-Institut für Solare Energiesysteme, New world record for solar cell efficiency at 46% French-German cooperation confirms competitive advantage of European photovoltaic industry, 2014.

Sasaki, K., Agui, T., Nakaido, K., Takahashi, N., Onitsuka, R., Takamoto, T., 2013. Development of InGaP/GaAs/InGaAs inverted triple junction concentrator solar cells. In: 9th International Conference on Concentrating Photovoltaics Systems, Miyazaki, Japan, pp. 22–25.

Shafarman, W.N., Paulson, P.D., 2005. Losses in $CuInSe_2$-based thin film monolithic tandem solar cells. In: Conference Record of the 31st IEEE Photovoltaic Specialists Conference, pp. 231–234.

Shafarman, W.N., Siebentritt, S., Stolt, L., 2010. Cu(In,Ga)Se_2 solar cells. In: Luque, A., Hegedus, S. (Eds.), Handbook of Photovoltaic Science and Engineering. John Wiley & Sons, Chichester, West Sussex, UK, pp. 546–599.

Smestad, G., Ries, H., 1992. Luminescence and current-voltage characteristics of solar cells and optoelectronic devices. Sol. Energy Mater. Sol. Cells 25, 51–71.

White, T.P., Lal, N.N., Catchpole, K.R., 2014. Tandem solar cells based on high-efficiency c-Si bottom cells: top cell requirements for >30% efficiency. IEEE J. Photovoltaics 4, 208–214.